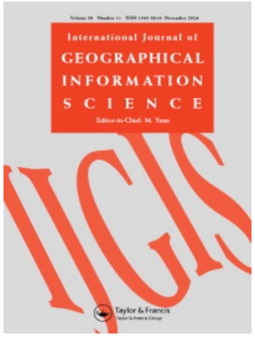

International Journal of Geographical Information Science

ISSN: (Print) (Online) Journal homepage: www.tandfonline.com/journals/tgis20

A new two-step estimation approach for retrieving surface urban heat island intensity and footprint based on urban-rural temperature gradients

Anqi Zhang & Chang Xia

INTERNATIONAL JOURNAL OF GEOGRAPHICAL INFORMATION SCIENCE
2024, VOL. 38, NO. 11, 2348–2378
https://doi.org/10.1080/13658816.2024.2385435

RESEARCH ARTICLE

A new two-step estimation approach for retrieving surface urban heat island intensity and footprint based on urban-rural temperature gradients

Anqi Zhang[a] and Chang Xia[b]

[a]School of Architecture and Art, Central South University, Changsha, China; [b]School of Public Administration, Hunan University, Changsha, China

ABSTRACT
Past decades have seen substantial efforts devoted to observing, assessing, and documenting the urban heat island (UHI) phenomenon. However, the discrepant criteria of non-urban references and ambiguous distinctions between urban and rural landscapes pose great challenges in measuring UHI magnitudes and spatial extents. This study goes beyond the conventional urban-rural dichotomy and introduces a new two-step approach based on the continuous transition of thermal environments along urban-rural gradients. The approach is applied to quantify Surface UHI (SUHI) intensities and footprints across 283 Chinese cities from 2005 to 2018 using multiple satellite-derived data sources. The results include: 1) The two-step approach avoids the limitations in subjective rural reference selections and provides reliable quantification of SUHI characteristics in various cities over time. 2) The SUHI footprints extracted by our approach are more reasonable than those obtained by two existing methods, with footprint ratios generally ranging within 0 – 6 times the urban area. 3) The two-step approach provides more concentrated estimates of SUHI intensity. Typically, ignoring heat sources in non-built-up areas can cause an overestimation of SUHI effect and misidentification of remote rural areas with high temperatures. Overall, the two-step approach enables more accurate estimates of SUHI effect, thereby facilitating policy-making for SUHI mitigation.

ARTICLE HISTORY
Received 15 November 2023
Accepted 24 July 2024

KEYWORDS
Surface urban heat island; estimation approach; footprint; intensity; China

1. Introduction

The accelerating urbanization processes and growing anthropogenic activities have drastically altered the Earth's atmospheric and surface features, thus affecting local energy balance and thermal climate in cities (Carrillo-Niquete *et al*. 2022; Eugenio Pappalardo *et al*. 2023; Grimm *et al*. 2008; Jones *et al*. 2008; Kalnay and Cai 2003; Xia *et al*. 2022; Zhang *et al*. 2021). Among the most evident aspects of human impacts, the urban heat island (UHI) effect is known as the phenomenon where urban centers have higher temperatures than adjacent, less-developed suburban and rural areas,

CONTACT Xia Chang xia2023@hnu.edu.cn

which has become a grave concern globally, especially in developing countries such as China (e.g. Cao *et al*. 2016; Carrillo-Niquete *et al*. 2022; Galán Díaz *et al*. 2023; Liu *et al*. 2023; Rizwan *et al*. 2008; Stone 2007; Zhao *et al*. 2014). The UHI effect poses significant challenges to the sustainable development of urban systems and serious threats to human health due to its negative impacts on air and water quality, strong associations with increases in energy consumptions, and substantial contributions to the rise of global warming and extreme heat events (e.g. Cao *et al*. 2018; Li *et al*. 2020; Zhao *et al*. 2018). Furthermore, the UHIs can exacerbate the harmful impacts of thermal stress on humans in both summer and non-summer seasons (Heaviside *et al*. 2017; Sadeghi *et al*. 2022; Schwarz *et al*. 2020). For example, heat-induced fatalities and diseases are often much greater in cities than in suburban or rural areas as a result of increased urban temperatures during heat waves (Royé *et al*. 2020; Xu *et al*. 2016). Therefore, there is a strong impetus to identify the UHIs and investigate their magnitudes and spatial extents.

Substantial efforts have been devoted to gaining a nuanced understanding of the UHI effect using both observed air temperatures monitored by ground weather stations (e.g. Oke *et al*. 2017) and surface temperatures derived from satellite images (e.g. Imhoff *et al*. 2010; Khan *et al*. 2023; Peng *et al*. 2012; Khan *et al*. 2023; Yao *et al*. 2024). In consideration of the sparse density of in-situ station networks and potential influences of very local weather conditions, satellite-derived land surface temperature (LST) has been increasingly and widely used to characterize spatial and temporal patterns of UHI effects across different cities or regions. Satellite-derived LST has advantages, such as continuous spatial coverage, sufficient resolution, and easy data access. On the other side, surface temperatures are more directly related to modifications in surface environments and urbanization processes (Phelan *et al*. 2015; Xiang *et al*. 2021), even though they are frequently higher and more variable than the concurrent air temperatures. Despite the fact that LST, as one of several types of temperatures, is not identical to human heat exposure and fails to capture the severity of urban heat, it can reflect important aspects of urban climate and be most relevant for characterizing regional UHIs (Turner *et al*. 2022). This study focuses on the surface UHI (SUHI) effect, which is characterized using LST and frequently just called the UHI, and deals with the estimates of the intensity and footprint of the SUHI effect.

While there is general evidence that SUHI intensity exhibits distinct temporal patterns, such as diurnal variation, comparative analysis on the spatial heterogeneity of SUHI effects across cities has been hindered by the loose and diverse definitions of urban versus non-urban extents and their temperature differences (Imhoff *et al*. 2010; Khan *et al*. 2023). The estimates of SUHI intensities and footprints in different studies can vary greatly due to the lack of an objective and commonly accepted method for identifying the temperatures or areas as unaffected references (Clinton and Gong 2013; Imhoff *et al*. 2010). For example, the SUHIs defined as temperature differences between urban and suburb areas could have lower intensity and a smaller footprint compared to those using urban-rural differences (Liu *et al*. 2023). The selection of non-affected references can significantly alter the SUHI measures, and the method of delineating non-urban areas can affect the amplitude and even direction of SUHI trends (Liu *et al*. 2023; Stewart 2011; Wang 2022). Furthermore, ecological contexts related to the functions and types of the broader landscape surface have significant influence on the identification of SUHI intensity and sign. The negative urban heat differential between the urban core and its surroundings, referred to as heat sinks or surface urban cold islands (SUCIs) in previous studies (e.g. Carnahan and Larson 1990; Clinton and Gong 2013; Khan *et al*. 2023), can be widely observed in cities surrounded by desert land and with semi-arid and arid climates. Significant daytime SUCI phenomenon can occur in high-rise and high-density cities if there is little or no anthropogenic heat (Yang *et al*. 2017). In fact, the SUHIs and SUCIs co-exist in many cities, which has been found to be associated with building forms and urban structures (Duan *et al*. 2019; Hamada and Ohta 2010). All these issues can lead to significant biases and challenges in estimating and comparing the SUHI effects across different geographic settings.

In previous studies on quantifying the SUHI effect, impervious surface areas and distances (e.g. buffer zones) are used to delineate the optimal urban boundary based on various classification criteria. The areas with surface temperatures above the threshold values (e.g. rural references) are identified as the footprint of SUHI (Imhoff *et al*. 2010; Peng *et al*. 2020; Quan *et al*. 2014; Si *et al*. 2022; Streutker 2003). For example, Zhou *et al*. (2014) distinguished high-density urban areas from adjacent suburban regions by employing a 50% threshold of built-up density (i.e. the proportion of impervious surface pixels) and a buffer zone equivalent to 100% of the urban area (i.e. the buffer matches the urban area in size). However, the temperature differences between urban and surrounding suburban areas can be significantly influenced by the selection of thresholds and distances (e.g. Liu *et al*. 2023; Wang 2022). Furthermore, many studies have indicated that the spatial extent of SUHI can extend to more than twice the size of urban areas (e.g. Peng *et al*. 2020; Yang *et al*. 2022). Thus, the equal-area or larger surroundings may not necessarily be far enough from the urban contour to truly represent the unaffected areas. It could be impossible to find a fixed buffer ring (e.g. 100% or 150% of urban areas) applicable for all cities with different geographic and socioeconomic settings. As Yang *et al*. (2022) suggested, part of these potential biases and uncertainties in SUHIs arise from overlooking the footprint of the SUHI effect. Hence, the combined estimates of SUHI intensity and footprint are essential.

The temperature features and SUHI profiles along the urban cross-sections have long been demonstrated to be mainly a result of the urban surface factors (i.e. land uses and distance to the city center) and independent of local weather conditions (Oke *et al*. 2017; Imhoff *et al*. 2010; Unger *et al*. 2001). In general, the magnitude of the SUHI effect significantly decreases with distance from urban areas, reaching peak values in city centers and dropping sharply at urban/rural boundaries (e.g. Oke 1987). Therefore, the temperature profiles along the urban-rural gradients have great potential to improve the estimates of the SUHI intensity and footprint (Krehbiel *et al*. 2016; Peng *et al*. 2020; Qiao *et al*. 2019; Zhang *et al*. 2004; Zhao *et al*. 2016; Zhou *et al*. 2015), but have not been widely utilized in current literature. Several attempts have been made to incorporate temperature profiles into SUHI estimates in various ways (Peng *et al*. 2020; Yang *et al*. 2022; Zhao *et al*. 2016; Zhou *et al*. 2015; Zhang *et al*. 2004). In particular, Zhou *et al*. (2015) created twelve buffers to analyze the UHI effect in the spatial extent around seven times the actual urban area. They quantified the footprint as the continuous areas emanating outward from urban core to rural areas with temperatures higher than the reference value (i.e. urban-rural temperature differences greater than zero). However, this method hypothesized that the SUHI footprints for the studied cities must be larger than the actual urban area. The SUHI estimates still suffered from the uncertainties associated with fixed and subjective definitions of unaffected references (Yao *et al*. 2024). The exponential model proposed by Zhang *et al*. (2004) and Yang *et al*. (2022) identified the SUHI footprints based on the distance at which temperature differences reach 95% of the asymptotic values. However, this model failed in cities where there was an insignificant exponential decrease trend of temperatures towards rural areas. Zhao *et al*. (2016) and Peng *et al*. (2020) applied the radius method to determine the threshold of SUHIs. The former considered the area of the critical circles as the footprint, while the latter used breakpoint values as the threshold for extracting SUHIs.

To date, there is still a lack of an integrated and systematic approach that combines temperature profiles and SUHI estimates remarkably well. Therefore, this study aims to propose a two-step SUHI estimation approach based on temperature profiles. It follows the geomorphic analogy with a typical SUHI as described by Oke (1987) in the analysis of horizontal temperature gradients. The study uses commonly acquired LST products from Aqua/MODIS (MYD11A1 V6) at a $1-\text{km}$ spatial resolution to measure SUHI intensities and footprints across 283 cities in China from 2005 to 2018. The study employs the proposed method along with two existing methods utilized in previous studies. China has witnessed an unprecedented pace of urbanization process during the past decades, accompanied by tremendous changes in urban landscapes and considerable variations in local climates (Grimm *et al*. 2008). As a result, the SUHI effect, particularly its intensities and footprints, would have varied dramatically. The primary objective is to identify similarities and deviations in the spatial patterns of SUHI across numerous urban cross-sections, laying the foundation for a more accurate estimation of SUHI and its intensity and spatial extent. This will serve as a basis for further in-depth analysis of the characteristics and mechanisms of the SUHI effect, and aid in the alleviation and mitigation of associated risks.

2. Temperature profiles and SUHI effect

The temperature in urban areas is often warmer than that in the surrounding rural areas. The exact magnitude and form of the SUHI effect vary across space and time due to local climatic, ecological, and urban attributes. As shown in Figure 1, Oke (1987) described the generalized cross-section of a typical SUHI in large cities using a geomorphic analogy. To simplify matters, a series of restrictions are imposed in the SUHI profiles: the heat island immediately after sunset, under cloudless skies, and with mild winds. The temperature gradients with distance away from urban center to rural area can be defined as follows: the center of an urban area exhibits a temperature peak where the maximum temperature is often observed. Most of the rest of the urban area is characterized by a warm 'plateau', where the temperature increases steadily but with a relatively weak horizontal gradient towards the urban core. The urban/rural boundary is expected to experience dramatic temperature drops from the urban area outward, analogized to a 'cliff' in the SUHI. The difference between the

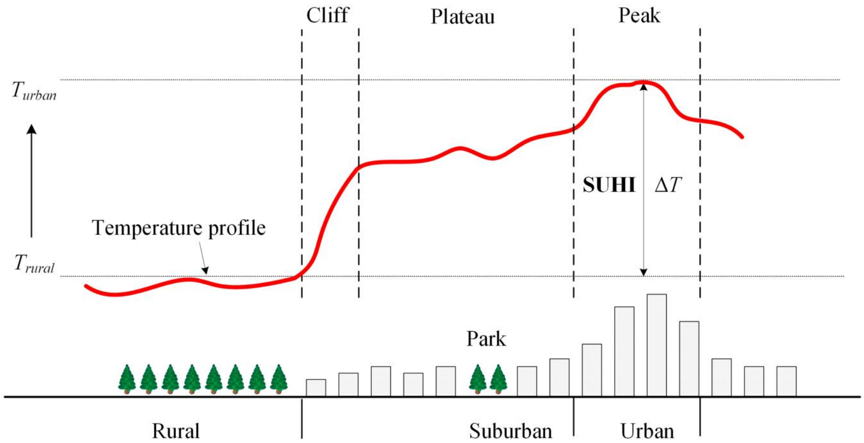

Figure 1. Generalized cross-section of a typical SUHI (adapted from Oke 1987).

temperature at the bottom of the cliff and the maximum urban temperature defines the intensity of a heat island (ΔT). The sharp horizontal temperature gradient in the urban-rural transition zone is one of the most prominent features in the SUHI profiles.

The decay in density of urban elements (e.g. built-up land, population, and economic activities) from the city center outward has been extensively studied across various research disciplines using different models, such as Gaussian and negative exponential functions (e.g. Batty & Sik Kim 1992; Clark 1951; Jiao 2015). This further demonstrates the aptness of the SUHI profiles. However, due to the lack of consideration for the temporal dimension, impacts of various climatic conditions, and city attributes, there may be similarities and deviations in the SUHI profiles for different cities or the same city at different times. For example, the uniformity of the SUHI profiles can be disrupted by the coexistence of high-density residential, commercial, and industrial built-up areas that generate and trap heat, as well as urban parks and water bodies that can mitigate heat island formation (e.g. Oke 1987; Cao *et al*. 2010). As a result of the presence of green and blue spaces, the cities' geographic or functional centers may not exactly be occupied by a heat 'peak'. Besides, urban spatial structure (e.g. monocentric and polycentric) can alter the SUHI profile, making it distinct from that observed under ideal conditions. More importantly, the simplified SUHI profile can vary noticeably throughout the day and night or under different weather conditions. All of these examples illustrate that the SUHI profiles can be influenced not only by differences in surface features between urban and rural areas but also by time-varying factors and the unique characters of cities.

The time-varying and city-specific factors cause huge biases and uncertainties in the estimates of the SUHI effect across different geographic contexts (Yang *et al*. 2023; *Zhang et al*. 2023). Nevertheless, despite the considerable modifications caused by the aforementioned factors, some recently published studies support that the temperature drops along urban cross-sections with profiles that remarkably align with typical characteristics if the SUHI effect is significant (Unger *et al*. 2001). Therefore, this study aims to propose a fundamental and effective approach to depict the SUHI intensity and footprint based on the profiles of urban-rural temperature variations. Compared with estimation

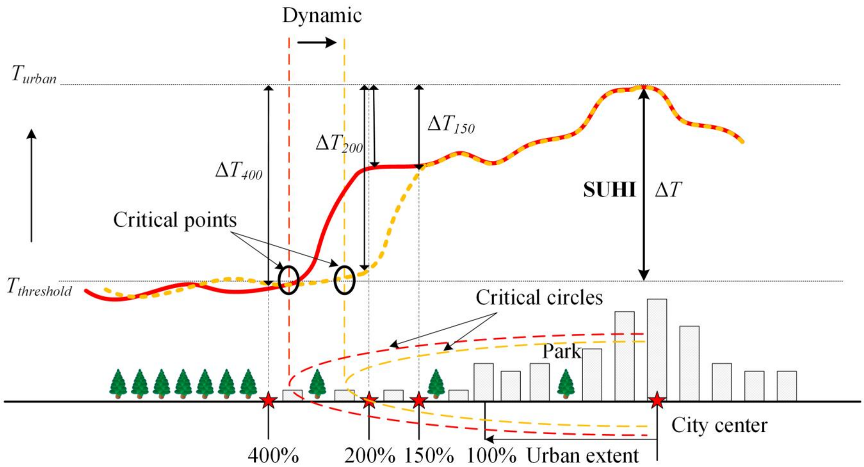

Figure 2. SUHI estimation based on temperature profiles and observations at fixed locations.

methods that heavily rely on observations at fixed locations (e.g. weather stations or pre-defined buffers), profiles are less affected by uncertainties associated with spatiotemporal changes in SUHIs. As shown in Figure 2, the critical points and critical circles in the gradient variation of urban-rural temperature can be crucial in quantifying the SUHI intensity and extracting the SUHI footprint in a dynamic way. Since there is no clear distinction between urban and rural landscapes, temperature profiles along the urban-rural gradients can offer a promising avenue to move beyond the traditional SUHI estimation relying on the urban-rural dichotomy (Wang 2022). Hence, the advantages of the two-step method also lie in the correction and dynamic identification of unaffected reference temperature based on the critical points and critical circles.

3. Methodology

3.1. Study area and data sources

The study examined the SUHI effect in 283 cities at and above the prefecture level in China, including 4 municipalities, 15 sub-provincial cities, and 264 prefecture-level cities (Figure 3). These cities were selected based on the administrative division in 2018, excluding some cities with missing data. It is noted that the spatial distribution of large cities and population in China is denser in the east and sparser in the west, resulting in a small number of prefecture-level and above cities in western provinces. Our study area covers most cities at the prefecture-level and above in China, with varying climate conditions, terrains, and development statuses, providing representative samples to validate our new approach. Given that temperature profiles can be affected by time-varying factors, this study compares the results of SUHI measures in different seasons to further validate the feasibility and applicability of our new approach. To identify the SUHI effect in these cities (i.e. administrative cities), multiple data sources are used and illustrated in the following section.

Remote sensing data are the primary data source used in the estimation of SUHI intensity and footprint, including data of LST, land cover, and digital elevation model

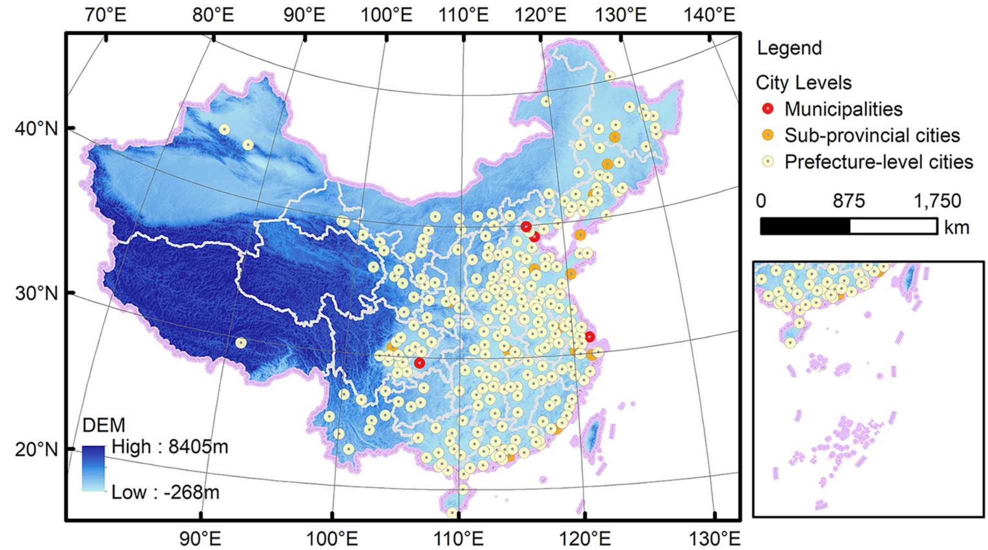

Figure 3. Location of the studied cities.
IJGIS remains strictly neutral with respect to jurisdictional claims on disputed territories and the naming conventions used in the maps included in the figure.

(DEM). The LST data used in this study is the 1 – km global daily LST/emissivity product (MYD11A1 V6) with both daytime and nighttime surface temperature bands provided by the NASA's Land Processes Distributed Active Archive Center (Wan *et al*. 2015). The seasonal and annual LSTs in the years of 2005, 2010, 2015, and 2018 were calculated based on the daily data from the Google Earth Engine (GEE) platform (Gorelick *et al*. 2017). For seasonal values, we computed spring (March – May), summer (June – August), autumn (September – November), and winter (December – February in the second year) mean values, whereas the annual mean is calculated from January to December in a year. The land cover data for the years of 2005, 2010, 2015, and 2018 were derived from the National Land-Use/Cover Database of China (NLUD-C), which were generated by manual visual interpretation based on Landsat TM images (Zhang *et al*. 2014), which include 6 primary classes and 25 subclasses and have classification accuracies exceeding 90% according to a nationwide field verification. The DEM data were provided by the Resource and Environment Science and Data Center (http://www.resdc.cn/), and resampled from the NASA's Shuttle Radar Topography Mission (SRTM) V4.1 products. Besides, the data for urban central and sub-central areas, identified using newly available points of interest data, were collected from Li *et al*. (2018), which is used in this study to extract the main centers and sub-centers.

3.2. A two-step SUHI estimation approach

In this study, a two-step SUHI estimation approach is proposed to estimate the SUHI intensity and extract the SUHI footprint based on the identification of critical points and critical circles in the SUHI profile. The major steps of this method are shown in Figure 4.

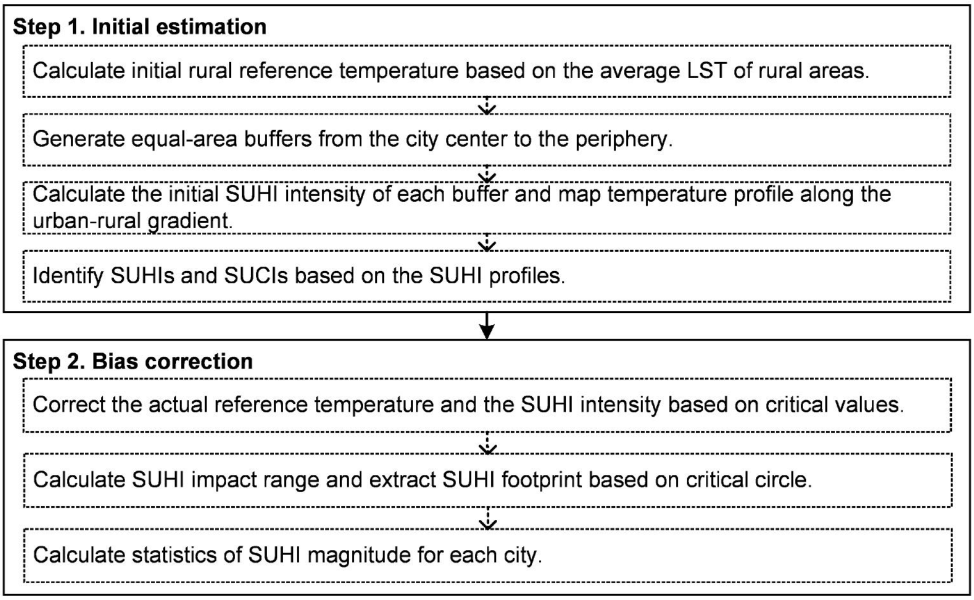

Figure 4. Flow chat of the two-step SUHI estimation approach.

Step 1, initial estimation of SUHI and urban-rural temperature profile.

1. Calculate the initial rural reference temperature (LST_{r0}). LST_{r0} is first defined using the average LST in rural areas. Here, rural areas are extracted based on land cover data and DEM data, and are defined as areas excluding urban built-up areas, water bodies, and mountainous regions within the city (Liu *et al*. 2023; Zhou *et al*. 2015). The extent of the city is defined according to the administrative divisions in 2018.
2. Generate equal-area buffers. Based on the geographical centroids of urban central areas, i.e. main centers, a large number of equal-area buffers are generated to cover the urban districts of each city[1]. The size of each buffer is determined as the lesser of 1/30 of the urban built-up area and 1/200 of the area of urban districts. These parameters are predefined by experiment to guarantee an adequate number of buffers in urban cores and suburban regions to capture the 'peaks' and 'cliffs' in temperature profiles. For sub-centers, the buffer size is reduced by half. The number of buffers is determined by 1.25 $\times$ the radius of the circle with an area equal to the urban districts and constrained by a maximum of 1000. Here, the urban built-up area for each city in 2005 is used to facilitate comparisons between different years (i.e. 2005, 2010, 2015, and 2018).
3. Calculate the initial SUHI intensity ($\widehat{SUHII}$) and map the temperature profile. To compare our approach with existing methods, this step is similar to the measures of SUHI customarily adopted in the literature to date. $\widehat{SUHII}$ is defined as the temperature differences between the LST of pixels and the LST_{r0}, based on the following equation:

$$\widehat{SUHII} = LST - LST_{r0} \tag{1}$$

The median $\widehat{SUHII}$ of the urban built-up and rural pixels within each buffer is considered as the buffer $\widehat{SUHII}$. Emanating outward from the urban core to the rural area, the $\widehat{SUHII}$ variations along the urban-rural gradient are mapped (refer to Figure 5).

4. Identify SUHIs and SUCIs. The identification of critical points and critical circles in the gradient variation of urban-rural temperature is key to the two-step SUHI estimation approach. Piecewise regression and manual interpretation are adopted to recognize the peaks, and critical points and circles of the SUHI profiles for different years. The presence of the SUHI and SUCI effects is identified based on the changing trend of the temperature profiles. If the temperature differences within the first quarter of the urban area are larger than zero, with the temperature 'peak' in the urban area and a temperature 'cliff' following it, the profile is classified as a SUHI. By contrast, a SUCI is identified if the temperature differences within the first quarter of the urban area are smaller than zero and increase outward from the urban core.

Step 2, bias correction and extension for the initial SUHI estimation.

5. Correct the actual reference temperature and SUHI intensity. For the temperature profiles identified as SUHIs in Step 1, the actual reference temperature is corrected to the median value of the LSTs of pixels in the critical circle (LST_c). Therefore, in the two-step SUHI estimation approach, the SUHI intensity for each pixel ($SUHII$) is estimated based on the following equation:

$$SUHII = LST - LST_c = \widehat{SUHII} - \widehat{SUHII}_C \tag{2}$$

where $\widehat{SUHII}_C$ refers to the $\widehat{SUHII}$ of the critical point. $\widehat{SUHII}_C$ *and* LST_c are determined by the change trend of the temperature profile and are unaffected by the urban-rural dichotomy. Such bias correction step can reduce spatial and temporal uncertainties, remove the influence of confounding factors, and facilitate cross-city and cross-time comparisons[2].

6. Calculate SUHI impact range and extract SUHI footprint. The SUHI footprint, i.e. the spatial extent of SUHI, refers to all pixels with $SUHII$ higher than zero (Imhoff *et al*. 2010; Peng *et al*. 2020; Quan *et al*. 2014; Streutker 2003), reflecting the spatial extent of SUHI. To avoid the influence of non-urban heat sources, the two-step method extracts SUHI footprints within the SUHI impact range, which is a buffer zone created from the edge of urban built-up areas[3]. The buffer radius (BR) is calculated based on following equations:

$$SUHIFPR = \frac{SUHIFP}{A} = \left(\frac{BR + \sqrt{A/\pi}}{\sqrt{A/\pi}}\right)^2 \tag{3}$$

$$BR_i = (\sqrt{SUHIFPR} - 1) * \sqrt{A_i/\pi} \approx (\sqrt{\widehat{FPR}} - 1) * \sqrt{A_i/\pi} \tag{4}$$

$$\widehat{FPR} = \frac{Area\ of\ buffers\ from\ city\ center\ to\ the\ critical\ circle}{Urban\ built\ up\ area\ from\ city\ center\ to\ the\ critical\ circle} \tag{5}$$

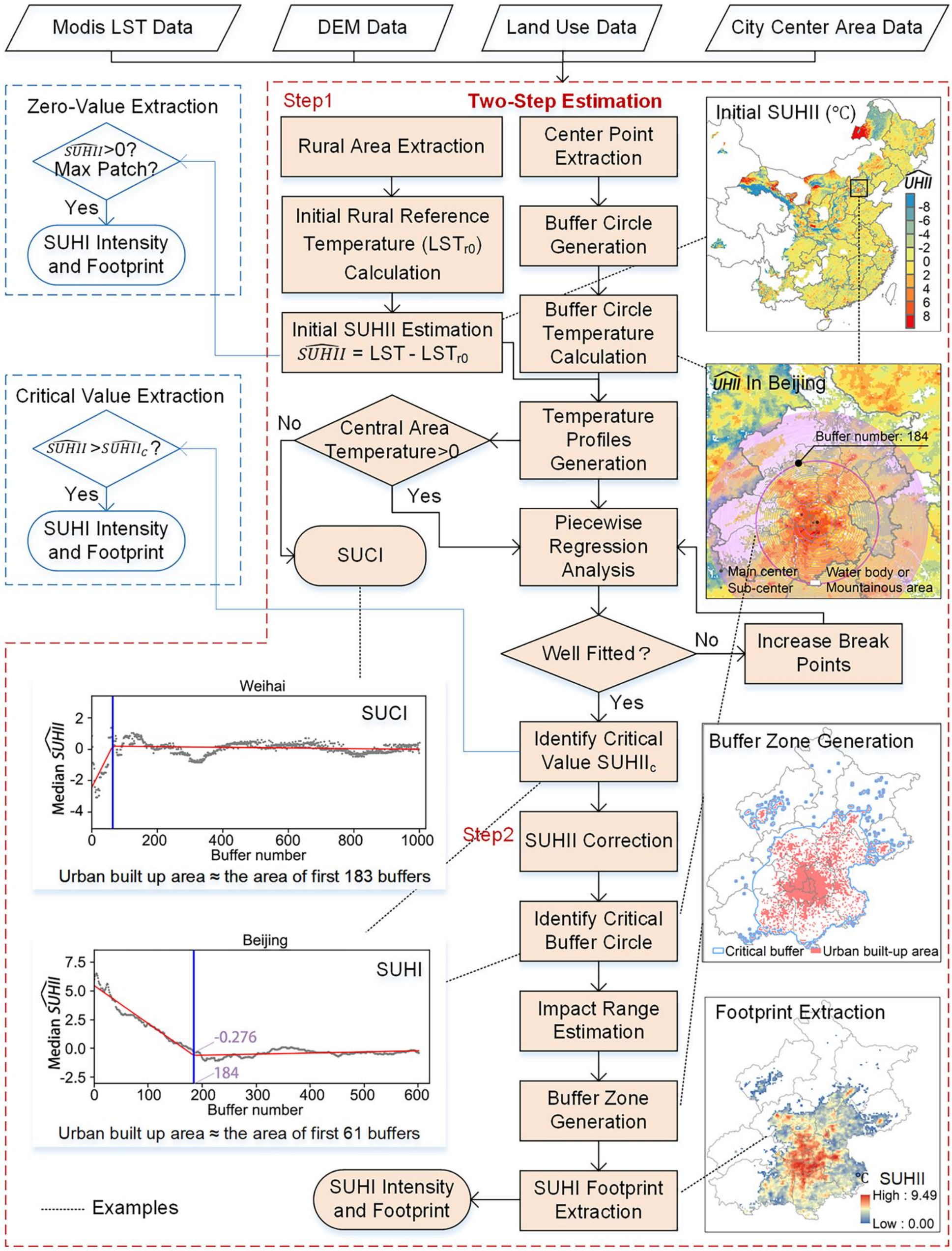

Figure 5. Procedures of the SUHI estimations.

where *SUHIFPR* refers to the SUHI footprint ratio, *SUHIFP* refers to the area of the SUHI footprint, *A* refers to the area of urban patches (i.e. continuous built-up areas), BR_i refers to the buffer radius for urban patch *i*, A_i refers to the area of urban patch *i*, and $\widehat{FPR}$ refers to the estimated value of *SUHIFPR*. The proportion of urban built-up areas within the buffer zone is assumed to be the same as the proportion within the critical circle. This is particularly relevant because the proportion of urban built-up areas, i.e. the reciprocal of *SUHIFPR*, is one of the most important factors in SUHI formation (Unger *et al*. 2001).

7. Calculate statistics of SUHI magnitude. The magnitude of SUHI intensity in each city is measured by *SUHII_mean* and *SUHII_max*, i.e. the mean and maximum *SUHII* of all pixels within the SUHI footprints, respectively. The magnitude of SUHI footprint in each city is measured by *SUHIFP* and *SUHIFPR*. *SUHIFPR* evaluates the actual extent of SUHI impacts (i.e. how larger areas are influenced by the SUHI effect compared to the actual urban size).

The detailed procedure to implement the two-step SUHI estimation in the empirical study is illustrated in Figure 5 and the subsequent sections.

It is noteworthy that the SUHIs and their impact ranges can vary substantially across space and time. The assessment and validation of SUHI estimation approaches based on various definitions, data, and measurements are necessary but complicated. In this study, we compare the proposed two-step SUHI estimates with the most widely used definition of urban-rural difference. The urban-suburban temperature difference is not included in the comparison due to the significant uncertainties and biases resulting from the lack of consideration of the spillover effect of the SUHI (Chun and Guhathakurta 2017; Liu *et al*. 2023; Zhou *et al*. 2015). Down to the root of the footprint concept, that is, the extent of increased temperature compared to rural references, three estimates of SUHI footprints can be obtained. One feasible method described in the literature (Zhou *et al*. 2015) quantifies the footprint as the continuous extent from the urban core to rural areas with a temperature difference significantly greater than zero value (termed as zero-value extraction hereafter). This common measure assumes that the observations from fixed locations represent an unaffected rural reference. The second method is adopted in some studies and is based on the transition points of the temperature profiles (Peng *et al*. 2020; Qiao *et al*. 2019), in which the locations are considered part of the SUHI footprints if the temperature is larger than the thresholds (Figure 5, critical value extraction). The two-step approach is expected to improve the above methods based on the SUHI impact extent and temperature profile. The classic Gaussian surface method proposed by Streutker (2003) is not considered here, as the UHI footprint is described as a two-dimensional spatial ellipse rather than the exact spatial extent of the UHI. Based on the extracted footprints based on the above three methods, four estimates of the SUHI magnitude (i.e. *SUHII_mean*, *SUHII_max*, *SUHIFP*, and *SUHIFPR*) can be acquired with temporal dynamics and spatial footprint of SUHI taken into account. We calculate the four SUHI indices for different time periods and cities.

4. Results

4.1. Quality assessment of the identified results based on two-step approach

An in-depth quality assessment is conducted to discuss the applicability and robustness of the two-step approach before its application. The temperature profiles across 283 cities revealed that the critical buffer circles in cities where the heat island effect occurs were generally consistent across different years but varied between day and night. Here, the probability of accurate estimates (*Prob*) for the critical buffer was assessed by comparison of the same periods across different years (Figure 6).

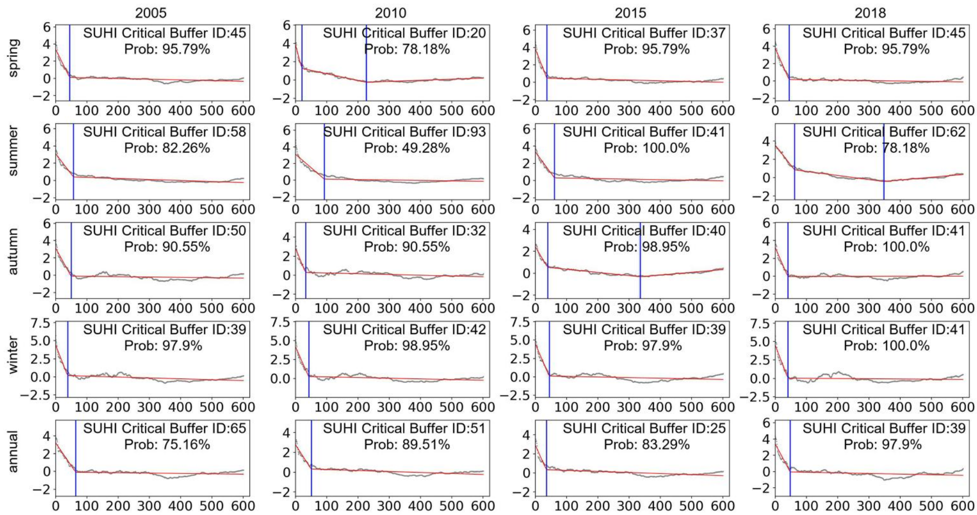

Figure 6. The nighttime SUHI identification results in Beijing based on the two-step estimation approach (x-axis: buffer number, unit of y-axis: °C).

Specifically, *Prob* was calculated based on the probability density of the normal distribution function, which was determined by the mean value and standard deviation of different years. Results with low *Prob* means the automatic recognition results of the algorithm might be unreliable, and further manual interpretation is needed. As shown in Figure 7, the accuracy of the results is lower during the day than at night, with the lowest accuracy observed during daytime in winter compared to other seasons. This may be because the nighttime SUHI footprints are usually more concentrated, and the SUHI characteristics in winter are relatively less obvious. Cases where the average critical buffer distance of the city is greater than 1.5 times the standard deviation were excluded when analyzing the characteristics of the SUHI. Overall, the two-step approach can provide a reliable quantification of the SUHI effect and its characteristics in various cities over time.

4.2. Urban heat and cool islands identification

Figure 8 shows the proportions of SUHI, SUCI, and uncategorized events during the day and night in different seasons and years, based on temperature changes with distance away from the city center. Among the 283 Chinese cities, more than 90% of cities experienced the SUHI effect in summer, followed by autumn, spring, and winter, whereas the SUCI effect exhibits an opposite seasonal trend, with no more than 4% of cities witnessing a SUCI in summer. The proportions of SUHIs and SUCIs vary significantly between day and night. The SUHI occurs more frequently at night and the SUCI occurs almost during the daytime. This is particularly obvious in winter, with around 34% and 82% heat islands and 39% and 6% cool islands during the day and night, respectively. In terms of the annual trend, daytime SUHIs show a slightly downward trend from 2005 to 2018, whereas the percentage of nighttime SUHIs has increased and reached its peak in 2015. The decrease in daytime SUHIs is found to be more

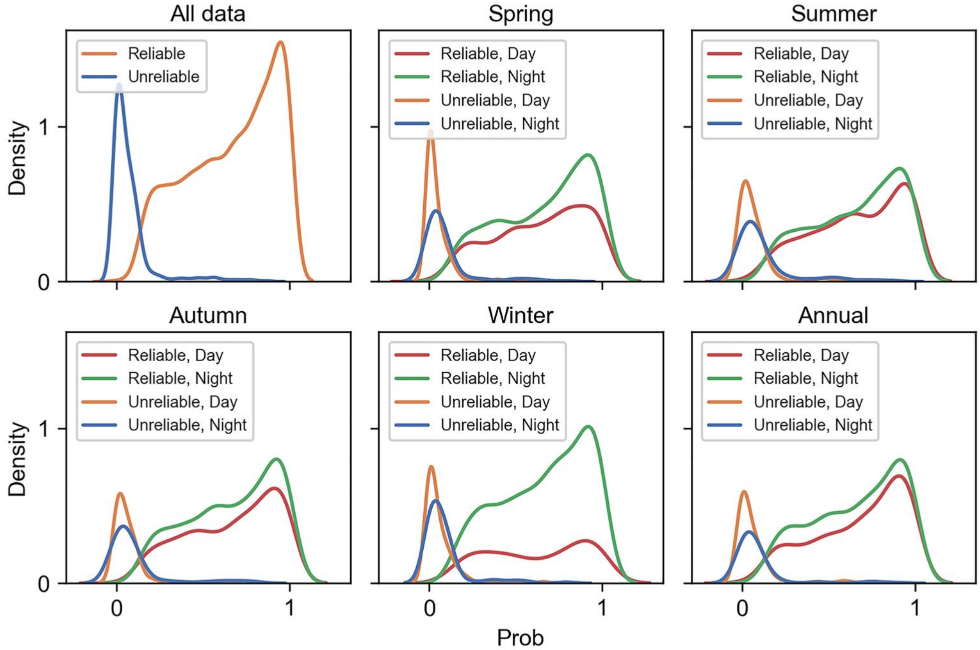

Figure 7. The quality of results based on the two-step estimation approach.

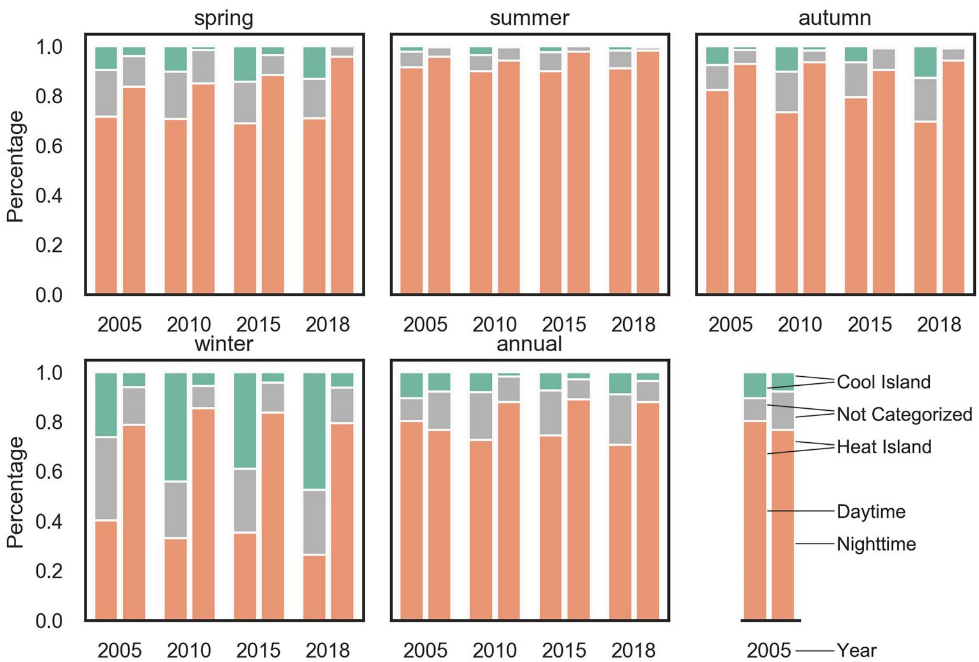

Figure 8. Statistics on the proportions of heat and cool islands.

concentrated in North China, where daytime SUCIs in non-summer seasons significantly increase due to the increased green infrastructures in city centers on one hand (Orkomi and Ameri 2024) and the higher elevation of newly built urban areas on the other hand (Liu *et al.* 2021). It is noted that the overall trend of SUHIs is still increasing during the study period.

Figures 9–13 present the spatial distribution of SUHIs and SUCIs for 283 cities in China. Regardless of the seasons and years, southern cities in China experience a significantly higher daytime SUHI effect compared to cities in the northern regions, whereas the cold island effect is predominantly observed during the day in North China. By contrast, nighttime SUCIs exhibit opposite distribution patterns, with almost all of them are found in the central and southern regions, especially in the Yangtze River Basin. Furthermore, daytime SUCIs occur much more frequently in winter than in other seasons. It can be found that the transition from SUCI in spring to SUHI in summer during the daytime occurs in some cities in North China. Subsequently, many northern cities experience a transition from daytime SUHI to daytime SUCI in autumn and winter. This may be related to the significant impact of humidity on SUHI, as daytime SUHI is stronger in a more humid climate. The reduction of vegetation and urban evaporation can cause urban dry islands, especially in mid-latitude cities with a water-

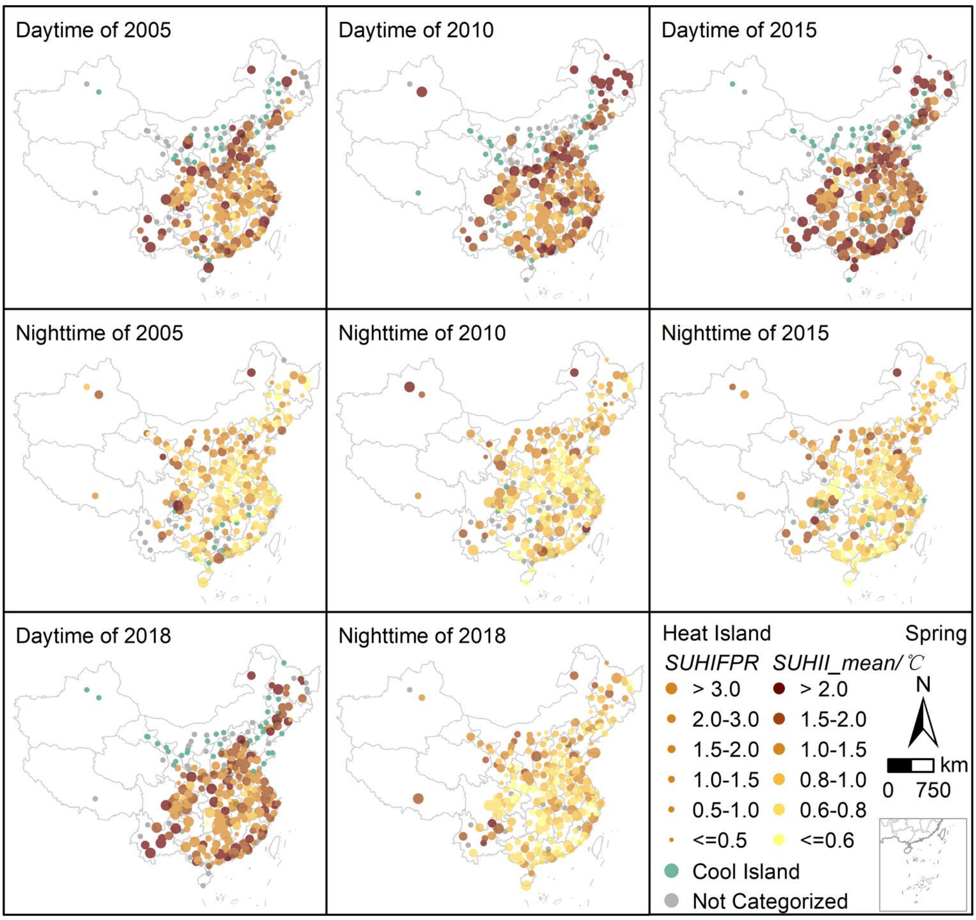

Figure 9. The distribution of heat and cool islands in spring.
IJGIS remains strictly neutral with respect to jurisdictional claims on disputed territories and the naming conventions used in the maps included in the figure.

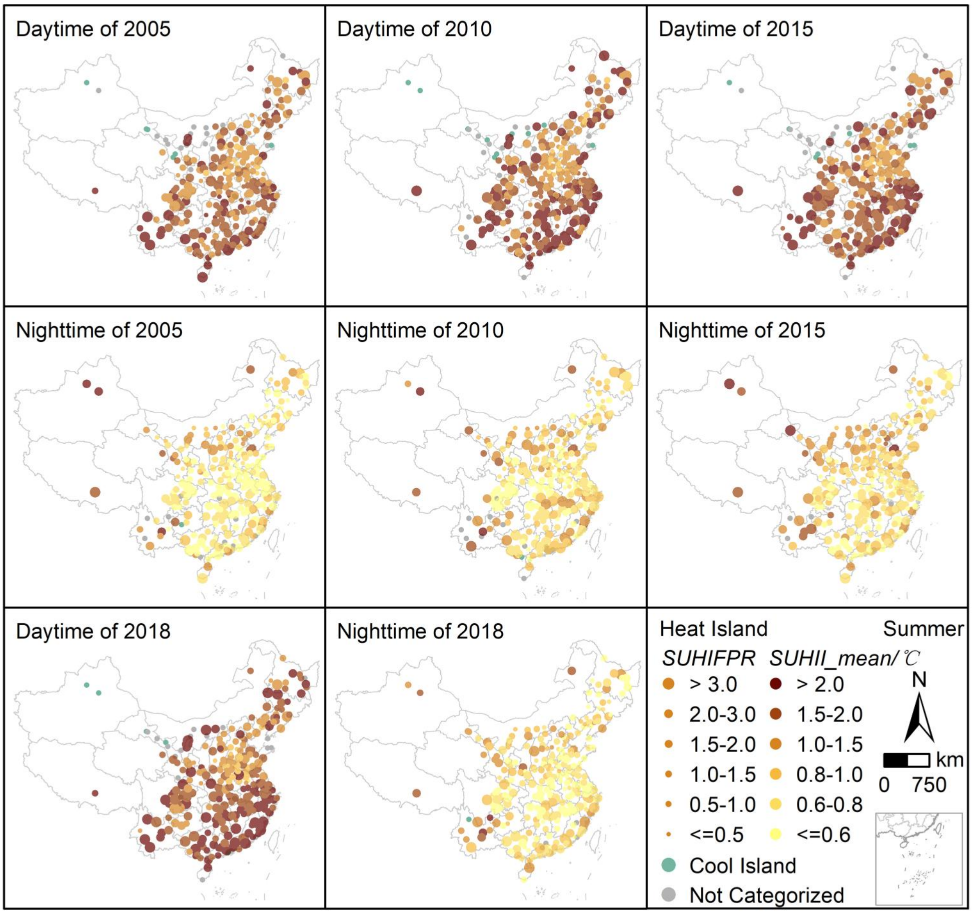

Figure 10. The distribution of heat and cool islands in summer.
IJGIS remains strictly neutral with respect to jurisdictional claims on disputed territories and the naming conventions used in the maps included in the figure.

limited evaporation climate, which can explain the prevalence of daytime SUCIs in North China during winter (Zhang *et al*. 2023). However, the SUHI effect occurs consistently in the northeast, southeast coastal, and southwestern areas regardless of the time of day, season, or year.

4.3. SUHI intensity and footprint

Based on the above identification results, the intensity and footprint of the SUHI effect are calculated using the proposed two-step estimation approach. In terms of SUHI intensity, most observations of *SUHII_mean* and *SUHII_max* (excluding outliers) fall within the ranges of 0 to 4 °C and 0.5 to 14 °C, respectively. The intensity during the daytime is, on average, 0.58 °C and 1.75 °C higher than that at night. Meanwhile, as shown in Figure 14, the high values of daytime *SUHII_mean* and *SUHII_max* are most concentrated in the northeastern and southeastern coastal cities and southwestern cities, but the nighttime values in north, northeast, and northwest China are the largest

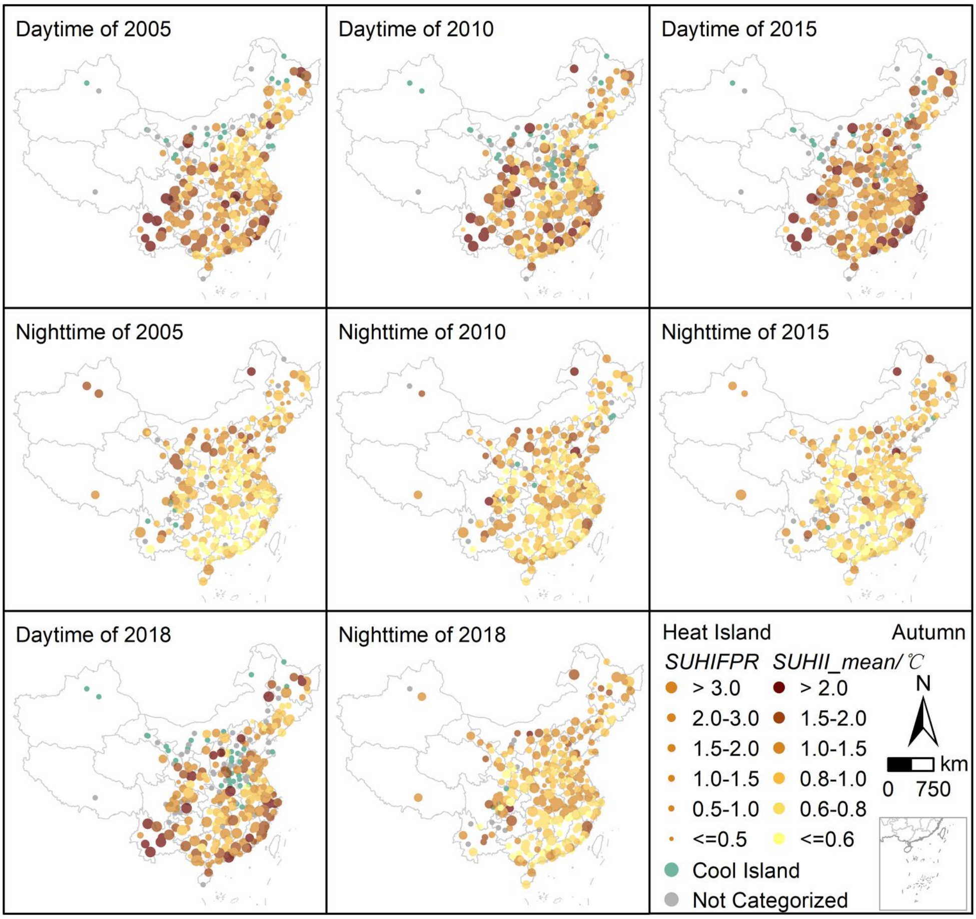

Figure 11. The distribution of heat and cool islands in autumn.
IJGIS remains strictly neutral with respect to jurisdictional claims on disputed territories and the naming conventions used in the maps included in the figure.

(Figure 15). Besides, most cities have higher daytime SUHI intensity in summer than in other seasons, particularly those located in the southern and southwestern regions, but the opposite is true for nighttime SUHI intensity (Figure 15).

The magnitude of SUHI footprints (i.e. *SUHIFPR*) ranges between 0 and 6 times the urban area in most cities after excluding the outliers, with daytime values, on average, 0.55 times greater than nighttime values. Meantime, as shown in Figure 14, the distributions of high *SUHIFP* or *SUHIFPR* values are similar during the day and night, which are concentrated in the eastern and southwestern regions, respectively. This implies that, the spatial area affected by the SUHI effect in eastern cities is large, while the impact range per unit of urban area in southwestern cities is large. In addition, *SUHIFPR* may not necessarily be the highest in summer compared to other seasons. However, *SUHIFPR* is larger in winter than in other seasons during the day, while the differences between seasons are less significant at night.

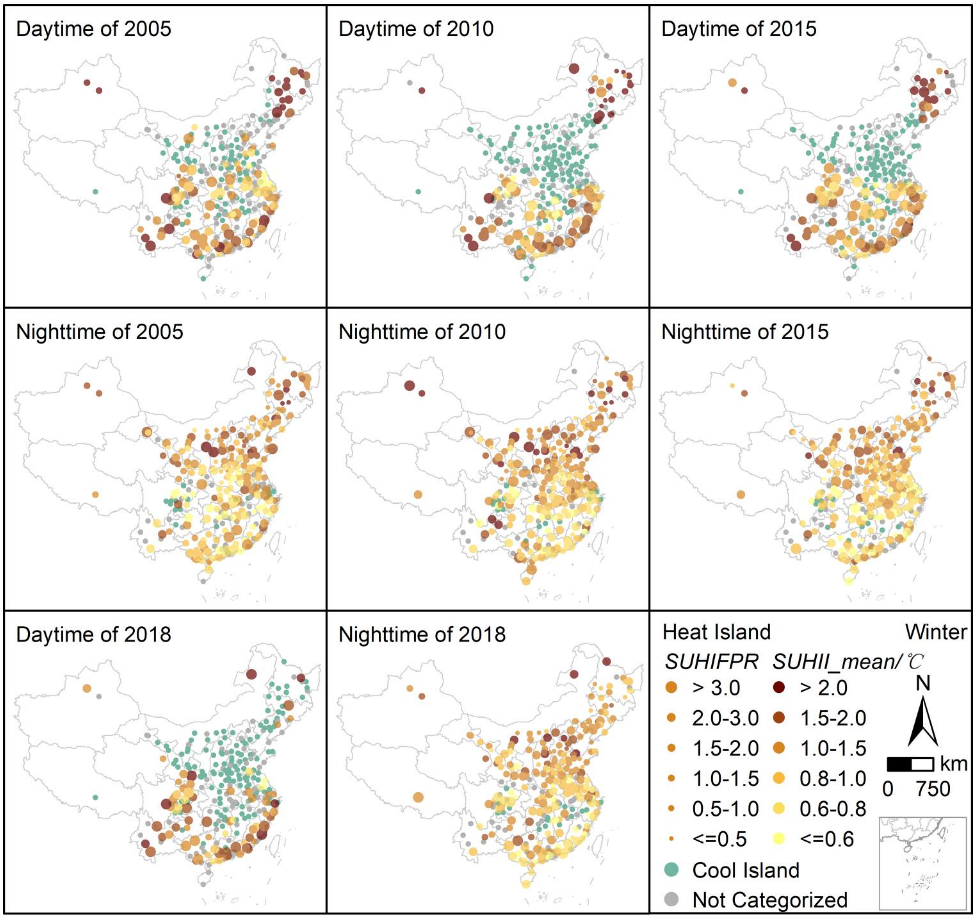

Figure 12. The distribution of heat and cool islands in winter.
IJGIS remains strictly neutral with respect to jurisdictional claims on disputed territories and the naming conventions used in the maps included in the figure.

5. Discussions

5.1. Benefits of the two-step SUHI estimation approach

The spread and temporal patterns of the SUHI intensity and footprint identified using the two-step approach and the critical value and zero-value extraction methods are compared. Figures 16–18 illustrate the boxplots of SUHI measures for all 283 cities in different years and seasons, with outliers excluded from the comparison. It was found that the footprints of SUHI extracted by the two-step approach are much smaller than the other two methods, with *SUHIFPR* between 0 – 6 times the urban area, and the median value of approximately 1.7 times during the day and 1.1 times during the night. Despite the similar estimated results, the two existing methods, especially zero-value extraction, obtained SUHI footprints that can reach up to more than 50 times the urban area of cities in China. This is not reasonable according to the findings of previous studies. For example, the footprints can be up to 5.5 and 6.5 times the urban size for the day and night, respectively, in the research of 32 Chinese cities from 2003 to 2012 by Zhou *et al.* (2015);

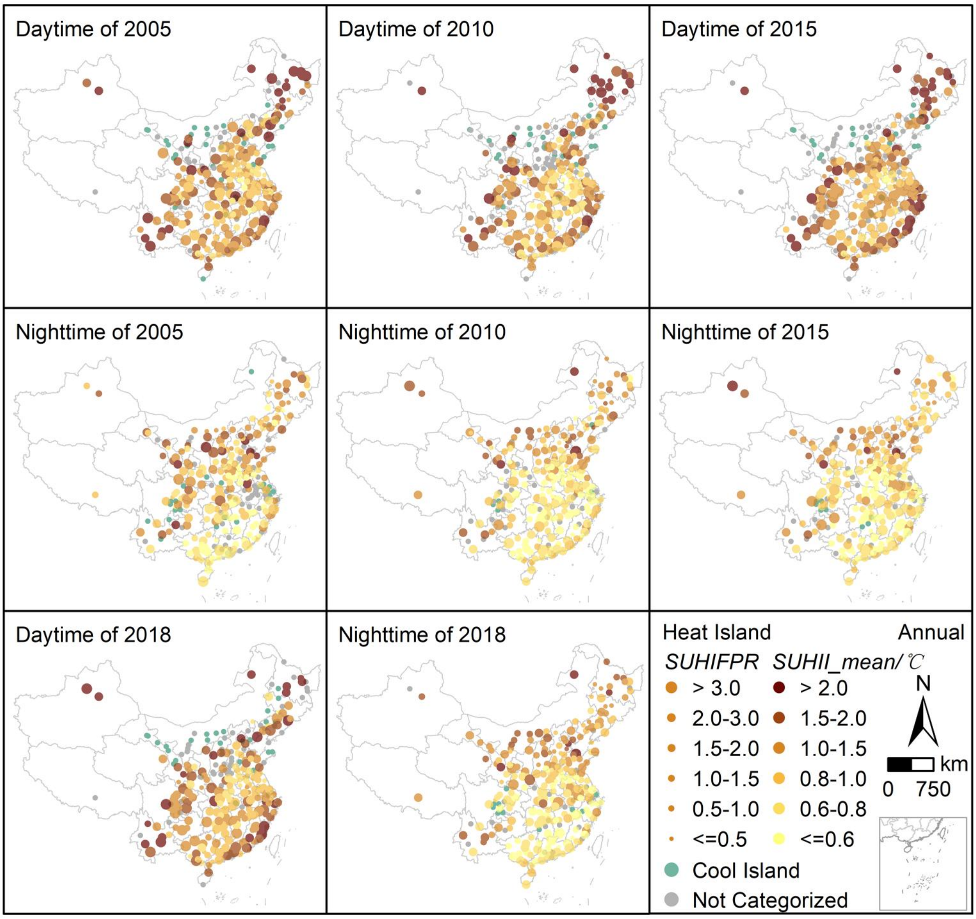

Figure 13. The distribution of heat and cool islands based on annual mean.
IJGIS remains strictly neutral with respect to jurisdictional claims on disputed territories and the naming conventions used in the maps included in the figure.

2.4 times the urban size in the research of eastern North America by Zhang *et al*. (2004); and smaller than twice the urban core area in the research of 141 cities in China from 2003 to 2020 by Hu *et al*. (2022). The median value of SUHI footprints is about 5 times (i.e. day: 5.4 times and night: 4.7 times) and 7 times (i.e. day: 6.7 times and night: 7.8 times) for the critical value extraction and zero-value extraction, respectively. In terms of the SUHI intensity, the two-step estimation technique and the other two methods show similar results; however, the two-step estimation technique tends to provide more concentrated estimates of SUHI intensity. These results suggest significant variations among various methods. Overall, the two-step technique provides more reasonable estimates of the area affected by the SUHI effect according to the estimations in existing literature.

Therefore, the two-step estimation approach is recommended in most cases, as it can provide a more accurate estimate for the SUHI footprint and intensity. Taking Beijing as an example, the zero-value extraction identifies the urban center as the SUHI footprint, but many urban areas are ignored, particularly those located far away

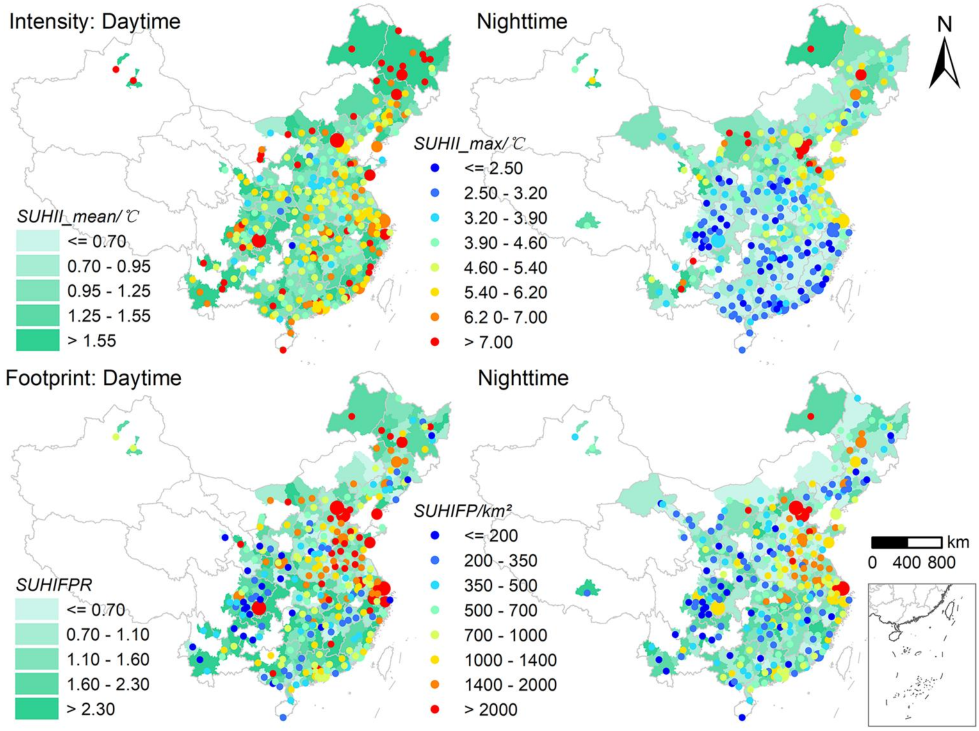

Figure 14. Spatial distribution of median SUHI intensities and footprints over the period of 2005–2018 and different seasons (point sizes represent the level of administrative regions, and the largest points are the municipalities directly under the central government, followed by sub-provincial cities and prefecture-level cities).
IJGIS remains strictly neutral with respect to jurisdictional claims on disputed territories and the naming conventions used in the maps included in the figure.

from the urban center (e.g. the Yanqing district, Figure 19). Meantime, the SUHI footprints, identified by the zero-value extraction, are determined by the definition of the rural area and its reference temperature. The critical value extraction method, without considering the impact range of the SUHI, often misidentifies some rural areas with high temperatures but far away from the urban area as the SUHI footprints.

Moreover, this new two-step estimation approach can be useful in some complicated cases. For example, multiple peaks may be found in the temperature profiles for both urban and rural areas, as 1) the sandy land, bare land, and grassland with low coverage may become the local hottest areas during the daytime (an example shown in Figure 20), and 2) the influences of the SUHI effect of surrounding big cities are large. In such cases, previous methods without considering heat sources and their impact ranges, usually identify much larger SUHI footprints compared to the actual impact extent (Figure 20).

5.2. SUHI characteristics and implications

Based on the identification of heat and cool islands, as well as the analysis of SUHI intensities and footprints, the spatiotemporal variations of SUHIs are demonstrated. In

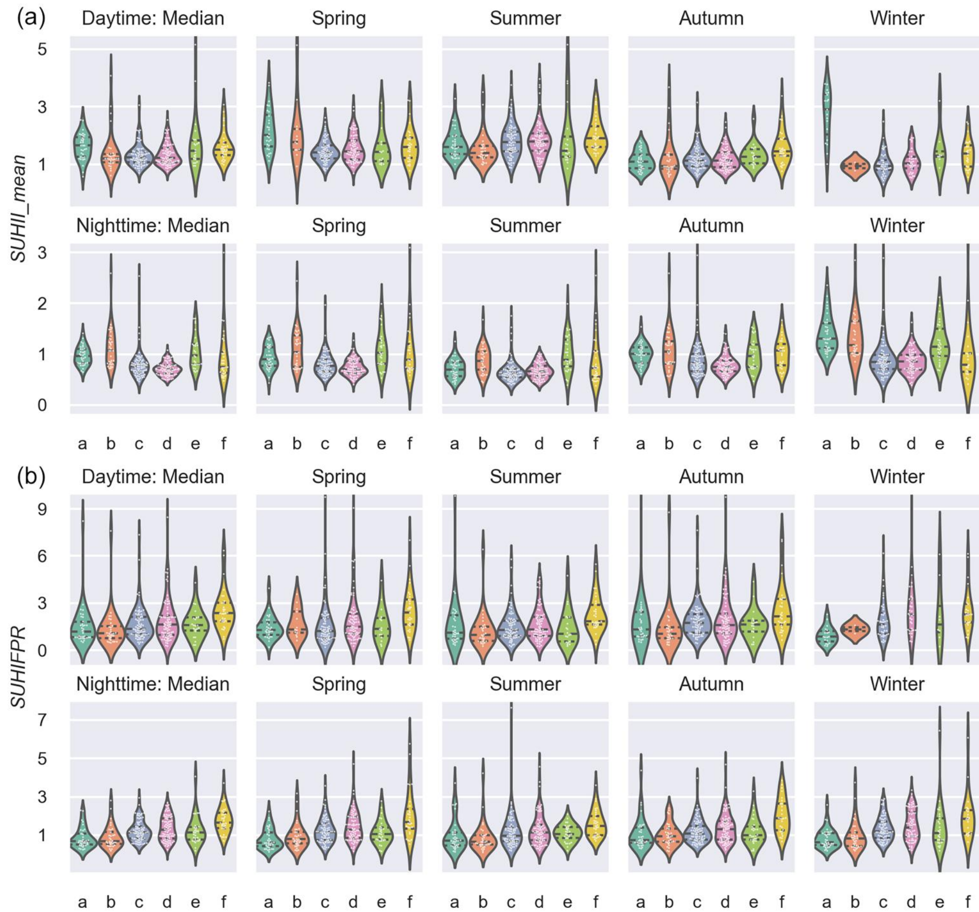

Figure 15. SUHI intensities and footprints over the period of 2005–2018 in different regions. (x-axis: a: Northeast China, b: North China, c: East China, d: Central South China, e: Northwestern China, f: Southwestern China; units of y-axis: (a) °C, (b) times the urban area).

terms of temporal variations, increasing trends in SUHI intensities and footprints (i.e. the magnitudes and spatial extents) over the period of 2005 – 2018 are observed in most cities (Figures 16–18). This trend has been linked to the rise in heat emissions and reduction in vegetation during urbanization processes in China (Yang *et al*. 2019; Zhou *et al*. 2014). The increase in greenery in rural areas may also be a significant factor driving the rise in daytime SUHI intensities (Yao *et al*. 2019). Given the increasing trends of SUHI intensity and footprint, it is essential to incorporate more green spaces, such as parks, gardens, and green rooftops, into urban planning, especially in areas covered by SUHI footprints. These spaces can help regulate temperature, reduce heat island effects, and improve overall urban climate resilience. Furthermore, some cities require special care. In cities with frequent SUHIs, Daqing and Yinchuan experienced a more than 90% rise in daytime *SUHII_mean*, and Tongchuan and Shangqiu saw an increase of over 65% in nighttime *SUHII_mean*. In these northern Chinese cities, conducting rigorous monitoring of SUHI intensity is essential to prevent its further growth. Meanwhile, Zhangzhou, Ganzhou, Chifeng, Huaihua, Nanping, and Chongqing,

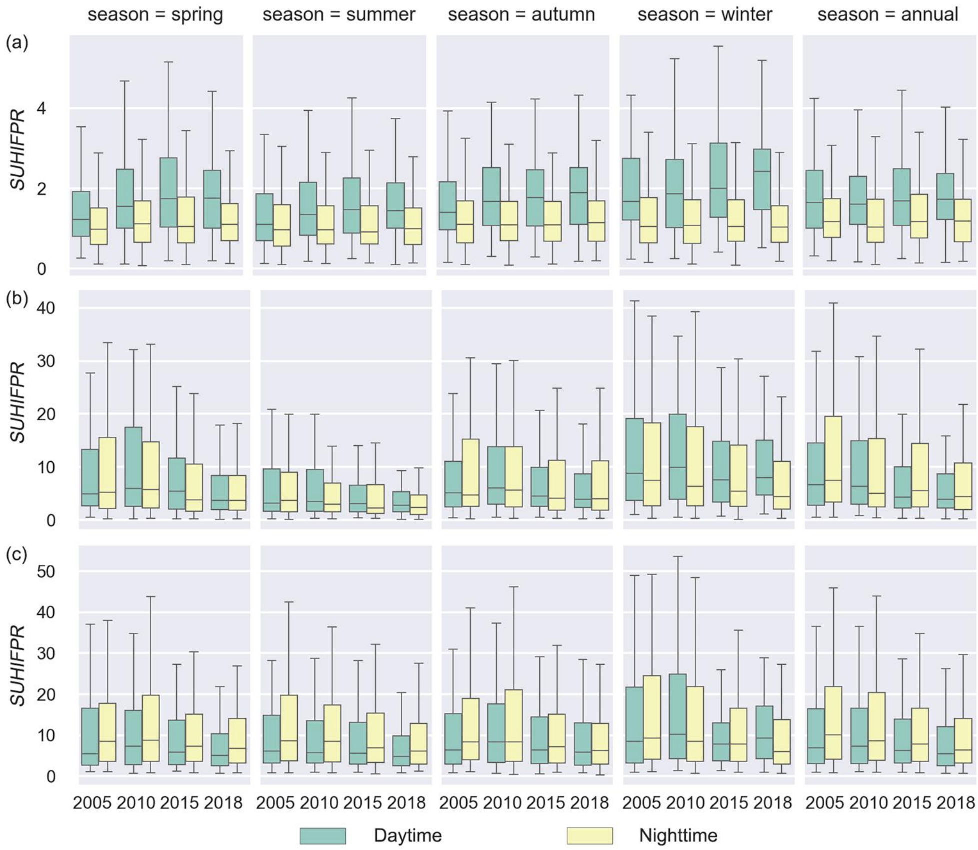

Figure 16. Statistics of the *SUHIFPR* values based on three different methods. (a-c: the results of the two-step estimation, critical value extraction, and zero-value extraction method, respectively; unit of y-axis: times the urban area).

primarily in southern China, had their daytime *SUHIFPR* increased by more than 250%. In contrast, Weinan, Hohhot, and Jiuquan in northwestern China, witnessed an over 190% increase in nighttime *SUHIFPR*. Prioritizing the design of urban and rural green belts is critical for these cities to reduce the spread and severity of SUHI effect.

In terms of the spatial distribution of SUHIs and SUCIs for 283 cities in China, the southern cities experience much more daytime SUHIs than the cities located in northern parts of China, regardless of the seasons and years. Conversely, the SUCIs during the day are predominantly observed in North China. This finding is in line with the recent report by Liu *et al.* (2021), who revealed that the increased green cover and higher elevations in newly developed urban areas, combined with the growing disparities in land development intensity during urban sprawl, led to a decrease in SUHI intensities in the North China Plain. In contrast, most cities in southern China experienced warmer temperatures in newly expanded urban areas, resulting in an overall rise in SUHI. Such variations in SUHI evolution across regions could also be partially attributed to background climates, which have the potential to alter the effects of land cover, such as green cover or impervious surfaces, on urban surface temperatures in different climate zones (Liu *et al.* 2023; Manoli *et al.* 2019; Naserikia *et al.* 2022).

Figure 17. Statistics of the *SUHII_max* values based on three different methods. (a-c: the results of the two-step estimation, critical value extraction, and zero-value extraction, respectively; unit of y-axis: °C).

In terms of the variations in SUHIs between day and night, daytime SUHIs have a lower proportion but higher intensity and footprint than nighttime SUHIs (Figure 8 and Figure 14). Specifically, SUHIs occur more frequently (i.e. higher SUHI occurrences) at night, which is in line with the research of Peng *et al*. (2018). Daytime footprints were found to be generally larger than nighttime ones based on the results of the two-step estimation approach (Figure 16). This finding contrasts with the results of the zero-value extraction method used in this study and the research by Zhou *et al*. (2015). However, Hu *et al*. (2022) and Yang *et al*. (2019) obtained similar findings based on analyses conducted in 141 and 302 Chinese cities, respectively. The possible reason is that the LST in suburban areas is slightly greater than LST in rural areas but significantly lower than LST in the city center. This causes different results from the zero-value extraction method and our two-step estimation approach (i.e. it identifies the inflection points). Besides, the daytime SUHI intensity is generally higher than the nighttime intensity (Figures 17, 18), which aligns with the findings of Peng *et al*. (2018) and Imhoff *et al*. (2010). However, it is worth noting that the SUHI intensities reported by Peng *et al*. (2018) exhibited contrasting trends in winter. To mitigate the higher daytime SUHI intensity, it is helpful to promote the use of cool building

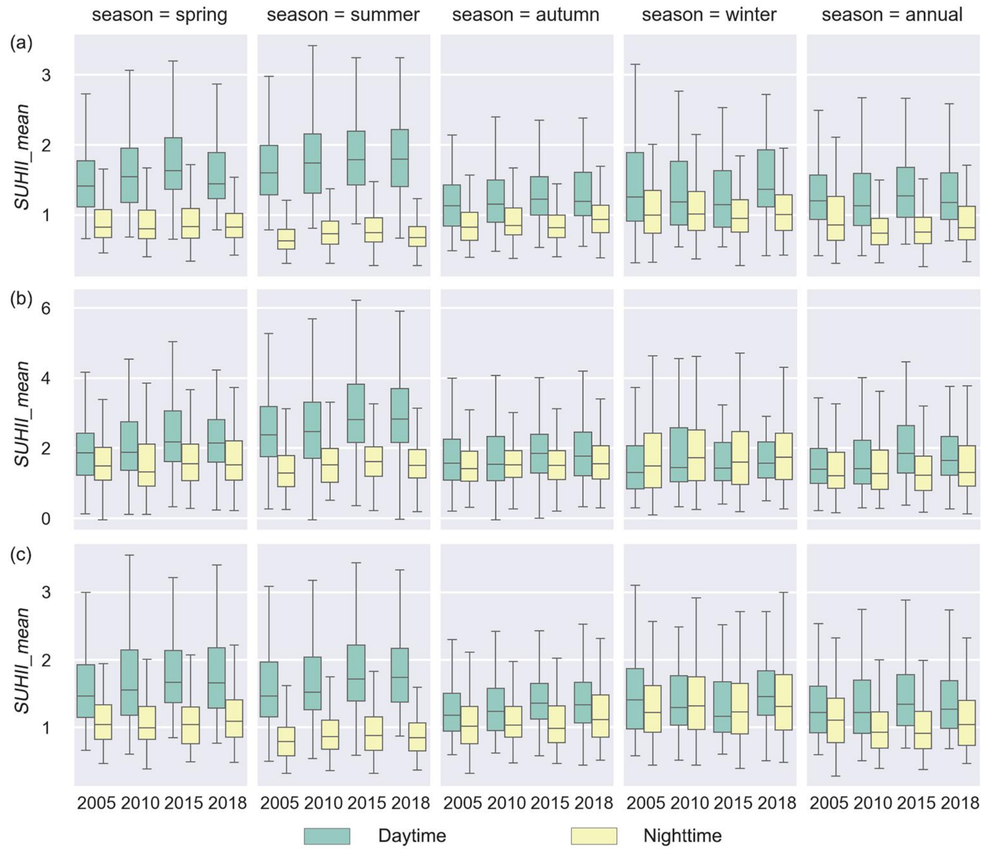

Figure 18. Statistics of the *SUHII_mean* values based on three different methods. (a-c: the results of the two-step estimation, critical value extraction, and zero-value extraction, respectively; unit of y-axis: °C).

materials such as reflective surfaces, and the urban design and renewal that can enhance natural ventilation and increase the building shading area (Wang and Shu 2020). These measures can reduce the heat absorbed by buildings and land surfaces, thereby lowering the overall temperature of the urban environments.

In terms of seasonal variations, the possibility of SUHI occurrence and the intensity of daytime SUHI are highest in summer (Figure 8 and Figure 14), as supported by the research of Peng *et al*. (2018). The seasonal variation of SUHI footprints in this study is different from Hu *et al*. (2022) and Yang *et al*. (2019). Our study reveals that the occurrence of the SUHI effect is obviously lower in winter compared to summer. However, for cities where the SUHI effect occurs in winter, their median SUHI footprint ratio and nighttime intensity in winter are larger than the median value for cities experiencing the SUHI effect in summer (Figure 14). This may be caused by the increasing heating demand, which leads to higher energy consumption, more waste heat production, and more severe air pollution. Therefore, it is necessary to encourage the construction of energy-efficient buildings and infrastructure to reduce energy consumption and minimize waste heat generation. This includes adopting passive solar design, improving insulation, and using energy-efficient heating systems. Given the higher daytime

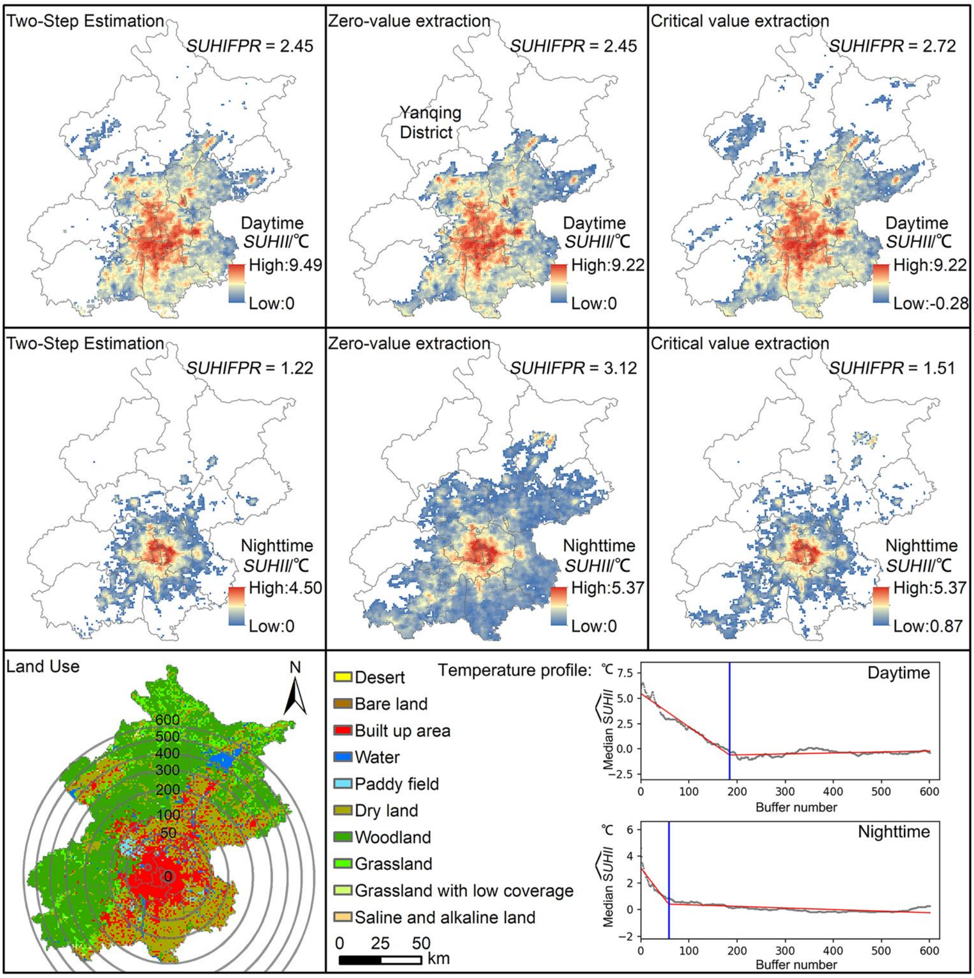

Figure 19. SUHI identification results in the summer of 2005 in Beijing.

SUHI intensity in summer and its impacts on urban dwellers, it is essential to develop targeted heat adaptation plans for vulnerable populations in urban areas with high SUHI intensity, such as the elderly and low-income households (Xia 2024). These plans may include the establishment of cooling centers, distribution of cooling aids, and public education on heat-related health risks. Besides, enforcing stricter air pollution regulations and investing in cleaner energy sources to reduce air pollution levels in urban areas can help limit the warming effects of air pollutants during winter.

5.3. Limitations

In the SUHI analysis, there are three sources of error: measurement error of LST, uncertainties related to the conceptual simplicity of the urban-rural dichotomy, and static measures caused by observations from fixed locations. The errors in deriving LST will partially cancel out in the SUHI calculation of temperature differences, even though a significant source of error may still exist between urban and rural surfaces. One major

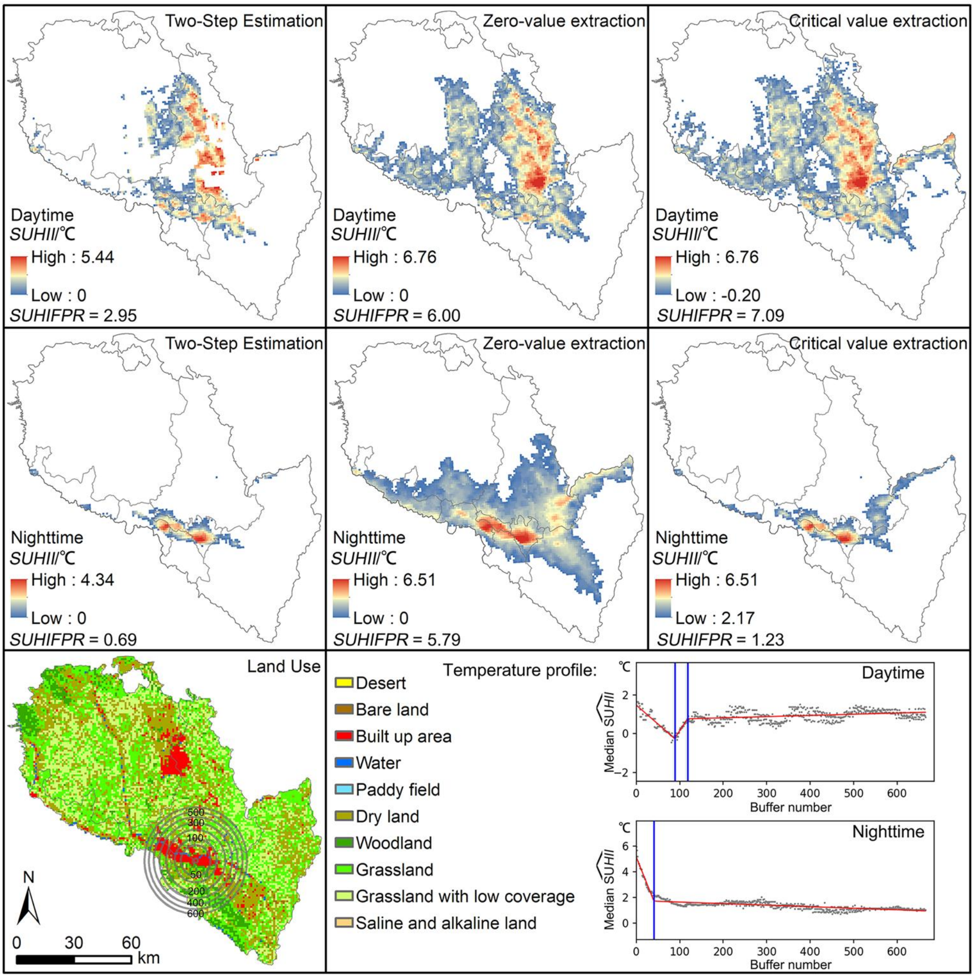

Figure 20. SUHI identification results in the summer of 2018 in Lanzhou.

advantage of the SUHI estimates considering spatial footprint, is that the magnitude of interest is not just the absolute contrast of the urban-rural thermal environment, but also the source areas of urban heat and the gradual transition from artificial to natural landscapes. This is important because rural surroundings can also contribute to the increased urban temperatures in some cases (it depends on urban-rural breezes and elevation), and there is a lack of clear demarcation between urban and rural environments (Wang 2022). However, SUHI estimates considering spatial footprint may still suffer from uncertainties related to the mismatch between the dynamic nature of SUHI footprint and static measurements based on fixed thresholds or locations. The two-step estimation approach could correct the errors described above that are common in existing studies.

Despite the advantages of the two-step estimation approach, there are still certain drawbacks to this approach. It can be, for example, sensitive to the model used to identify critical thresholds and the number of buffers generated to cover the study area. Therefore, the new method is not recommended in some cases. For example, in small urban built-up areas and with coarse LST datasets (e.g. urban areas covered by a limited number of pixels), it can be challenging to characterize the temperature changes from urban to rural areas. Besides, the method may not be suitable if the temperature profile shows a smooth or linear trend without any critical points.

Furthermore, uncertainties remain in the estimated SUHI intensity and footprint in this study. First, we identified the location of the urban-rural temperature 'cliff' and assumed that the proportion of urban built-up areas is key to the formation of SUHI effect. The SUHI footprint was extracted from the buffer zones created at the edge of the urban built-up area. However, the spatial distribution of source areas contributing to urban heat might not be homogeneous in cities. This suggests that we may not capture all the areas affected by SUHI in some cases. Second, the average SUHI intensity can be influenced by potential biases in the estimation of the SUHI footprints. Finally, the median temperature of the buffer rings was used to map the SUHI profile in this analysis, and piecewise regression was adopted to recognize critical points in the profiles. Future studies can explore whether the urban-rural temperature gradient can be influenced by the choice of characteristic value, such as mean or mode, as well as the selection of methods for identifying transition points. Furthermore, employing more accurate and high-resolution gap-free LST data may help reduce uncertainties associated with SUHI estimation (Yang *et al*. 2023; Yao *et al*. 2021, 2023). The use of local climate zones can provide more information about how the urban three-dimensional layout and structure influence the SUHI. These limitations stress the need for more efforts to conceptualize and measure the intensity and extent of SUHI in future studies.

6. Conclusion

The SUHI phenomenon has become increasingly prevalent in Chinese cities in recent years as a result of rapidly growing urban populations and industrialization. The accurate SUHI estimate helps in understanding the spatiotemporal variation of SUHI effect. However, these estimates are hindered by imprecise criteria for non-urban references and a vague distinction between urban and rural landscapes. In this study, we proposed a two-step SUHI estimation approach based on the urban-rural temperature profile and the geomorphic analogy with a typical SUHI. The approach was applied to extract spatial footprints of SUHI in 283 cities in China during 2005-2018 and identify the SUHIs and their magnitudes. Through a comparative analysis, the newly proposed two-step SUHI estimation approach is found to have advantages in reducing possible biases and uncertainties in SUHI measures and obtaining concentrated estimates of SUHI footprints (i.e. SUHI footprints are $0-6$ times the urban area) and intensities (i.e. the SUHI mean intensity ranges between $0-4\,^{\circ}C$ and the maximum intensity ranges between $0.5-14\,^{\circ}C$). The findings indicate that most cities in China experience a summer SUHI effect, with a general upward trend from 2005 to 2018. Southern cities are particularly prone to daytime SUHI, with mean and maximum intensities during the day averaging $0.58\,^{\circ}C$ and $1.75\,^{\circ}C$ higher than those at night. The two-step estimation approach used to extract SUHI footprints produces significantly smaller footprints compared to two existing methods and enables more accurate assessments of the changing patterns, mechanisms, and consequences of the SUHI effect, thereby aiding in the development of effective policies for mitigation.

Notes

1. City districts (*shiqu*) in China constitute the urban core of prefecture-level administrative units, which include urban and suburban districts (*chengqu* and *jiaoqu*) but not suburban counties.
2. Please note that the static rural reference values can be impacted by landscape changes in rural areas resulting from urban sprawl or plant growth (Wang 2022). These values are sensitive to the ecological context (*e.g.,* desert shrub-land) and the measurement of surrounding rural areas (*i.e.,* how far is enough from the urban core to represent the unaffected area).
3. The reason for creating a buffer zone from the edge of urban built-up areas is that the critical circle is unable to represent the actual range of SUHI due to the irregular shapes of urban areas (Peng *et al*. 2020).

Acknowledgments

We sincerely thank the editors and four anonymous reviewers for their helpful comments. We would also like to extend our thanks to Dr. Weifeng Li at The University of Hong Kong for his valuable suggestions and support for this research.

Disclosure statement

No potential conflict of interest was reported by the author(s).

Funding

This work was financially supported by the National Social Science Fund of China (Grant No. 23CTJ022), the Fundamental Research Funds for the Central Universities of Hunan University (Grant No. 531118010906), and the Fundamental Research Funds for the Central Universities of Central South University (Grant No. 502044010).

Notes on contributors

Anqi Zhang is an Assistant Professor in the School of Architecture and Art at Central South University, Changsha, Hunan, China. Her research interests include urban morphology, spatial analytics, and applications of geographical open data in urban and environmental studies. In this paper, her contributions include model implementation, visualization, writing and revision of the original manuscript.

Chang Xia is an Associate Professor in the School of Public Administration at Hunan University, Changsha, Hunan, China. His research interests include urban modelling, urban morphology, hazard adaptation, and applications of GIS and big data. In this paper, his contributions include conceptualization of the research idea, writing and revision of the original manuscript.

Data and codes availability statement

The data, codes, and instructions that support the findings of this study are available with the identifier(s) at the private link: https://doi.org/10.6084/m9.figshare.24760761.

References

Batty, M., and Sik Kim, K., 1992. Form follows function: reformulating urban population density functions. *Urban Studies*, 29 (7), 1043–1069.

Cao, C., *et al.*, 2016. Urban heat islands in China enhanced by haze pollution. *Nature Communications*, 7 (1), 12509.

Cao, Q., *et al.*, 2018. Impacts of future urban expansion on summer climate and heat-related human health in eastern China. *Environment International*, 112, 134–146.

Cao, X., *et al.*, 2010. Quantifying the cool island intensity of urban parks using ASTER and IKONOS data. *Landscape and Urban Planning*, 96 (4), 224–231.

Carnahan, W.H., and Larson, R.C., 1990. An analysis of an urban heat sink. *Remote Sensing of Environment*, 33 (1), 65–71.

Carrillo-Niquete, G.A., *et al.*, 2022. Characterizing spatial and temporal deforestation and its effects on surface urban heat islands in a tropical city using Landsat time series. *Landscape and Urban Planning*, 217, 104280.

Chun, B., and Guhathakurta, S., 2017. Daytime and nighttime urban heat islands statistical models for Atlanta. *Environment and Planning B: Urban Analytics and City Science*, 44 (2), 308–327.

Clark, C., 1951. Urban population densities. *Journal of the Royal Statistical Society. Series A (General)*, 114 (4), 490–496.

Clinton, N., and Gong, P., 2013. MODIS detected surface urban heat islands and sinks: Global locations and controls. *Remote Sensing of Environment*, 134, 294–304.

Duan, S., *et al.*, 2019. The impact of building operations on urban heat/cool islands under urban densification: A comparison between naturally-ventilated and air-conditioned buildings. *Applied Energy*, 235, 129–138.

Eugenio Pappalardo, S., Zanetti, C., and Todeschi, V., 2023. Mapping urban heat islands and heat-related risk during heat waves from a climate justice perspective: A case study in the municipality of Padua (Italy) for inclusive adaptation policies. *Landscape and Urban Planning*, 238, 104831.

Galán Díaz, J., Gutiérrez-Bustillo, A.M., and Rojo, J., 2023. Influence of urbanisation on the phenology of evergreen coniferous and deciduous broadleaf trees in Madrid (Spain). *Landscape and Urban Planning*, 235, 104760.

Gorelick, N., *et al.*, 2017. Google Earth Engine: Planetary-scale geospatial analysis for everyone. *Remote Sensing of Environment*, 202, 18–27.

Grimm, N.B., *et al.*, 2008. Global change and the ecology of cities. *Science (New York, N.Y.)*, 319 (5864), 756–760.

Hamada, S., and Ohta, T., 2010. Seasonal variations in the cooling effect of urban green areas on surrounding urban areas. *Urban Forestry & Urban Greening*, 9 (1), 15–24.

Heaviside, C., Macintyre, H., and Vardoulakis, S., 2017. The urban heat island: implications for health in a changing environment. *Current Environmental Health Reports*, 4 (3), 296–305.

Hu, J., *et al.*, 2022. Spatial patterns and temporal variations of footprint and intensity of surface urban heat island in 141 China cities. *Sustainable Cities and Society*, 77, 103585.

Imhoff, M.L., *et al.*, 2010. Remote sensing of the urban heat island effect across biomes in the continental USA. *Remote Sensing of Environment*, 114 (3), 504–513.

Jiao, L., 2015. Urban land density function: A new method to characterize urban expansion. *Landscape and Urban Planning*, 139, 26–39.

Jones, P.D., Lister, D.H., and Li, Q., 2008. Urbanization effects in large-scale temperature records, with an emphasis on China. *Journal of Geophysical Research: Atmospheres*, 113 (D16), D16122.

Kalnay, E., and Cai, M., 2003. Impact of urbanization and land-use change on climate. *Nature*, 423 (6939), 528–531.

Khan, M.S., Ullah, S., and Chen, L., 2023. Variations in surface urban heat island and urban cool island intensity: a review across major climate zones. *Chinese Geographical Science*, 33 (6), 983–1000.

Krehbiel, C.P., Jackson, T., and Henebry, G.M., 2016. Web-enabled Landsat data time series for monitoring urban heat island impacts on land surface phenology. *IEEE Journal of Selected Topics in Applied Earth Observations and Remote Sensing*, 9 (5), 2043–2050.

Li, J., Long, Y., and Dang, A., 2018. Live-Work-Play Centers of Chinese cities: Identification and temporal evolution with emerging data. *Computers, Environment and Urban Systems*, 71, 58–66.

Li, Y., *et al.*, 2020. On the influence of density and morphology on the Urban Heat Island intensity. *Nature Communications*, 11 (1), 2647.

Liu, H., *et al.*, 2021. Impacts of the evolving urban development on intra-urban surface thermal environment: evidence from 323 Chinese cities. *The Science of the Total Environment*, 771, 144810.

Liu, H., *et al.*, 2023. Influence of non-urban reference delineation on trend estimate of surface urban heat island intensity: A comparison of seven methods. *Remote Sensing of Environment*, 296, 113735.

Manoli, G., *et al.*, 2019. Magnitude of urban heat islands largely explained by climate and population. *Nature*, 573 (7772), 55–60.

Naserikia, M., *et al.*, 2022. Background climate modulates the impact of land cover on urban surface temperature. *Scientific Reports*, 12 (1), 15433.

Oke, T.R., 1987. *Boundary layer climates*. 2nd ed. London: Methuen.

Oke, T.R., *et al.*, 2017. *Urban climates*. Cambridge: Cambridge University Press.

Orkomi, A.A., and Ameri, M., 2024. Investigating the intensity of urban heat island and the impacts of local climate using verified WRF data: A case study of Rasht, Northern Iran. *Sustainable Cities and Society*, 106, 105405.

Peng, J., *et al.*, 2018. Spatial-temporal change of land surface temperature across 285 cities in China: An urban-rural contrast perspective. *The Science of the Total Environment*, 635, 487–497.

Peng, J., *et al.*, 2020. Quantifying spatial morphology and connectivity of urban heat islands in a megacity: A radius approach. *The Science of the Total Environment*, 714, 136792.

Peng, S., *et al.*, 2012. Surface urban heat island across 419 global big cities. *Environmental Science & Technology*, 46 (2), 696–703.

Phelan, P.E., *et al.*, 2015. Urban Heat Island: Mechanisms, Implications, and Possible Remedies. *Annual Review of Environment and Resources*, 40 (1), 285–307.

Qiao, Z., *et al.*, 2019. Determining the boundary and probability of surface urban heat island footprint based on a logistic model. *Remote Sensing*, 11 (11), 1368.

Quan, J., *et al.*, 2014. Multi-temporal trajectory of the urban heat island centroid in Beijing, China based on a Gaussian volume model. *Remote Sensing of Environment*, 149, 33–46.

Rizwan, A.M., Dennis, L.Y.C., and Liu, C., 2008. A review on the generation, determination and mitigation of Urban Heat Island. *Journal of Environmental Sciences*, 20 (1), 120–128.

Royé, D., *et al.*, 2020. Heat wave intensity and daily mortality in four of the largest cities of Spain. *Environmental Research*, 182, 109027.

Sadeghi, M., *et al.*, 2022. The health benefits of greening strategies to cool urban environments–A heat health impact method. *Building and Environment*, 207, 108546.

Schwarz, L., *et al.*, 2020. The health burden of fall, winter and spring extreme heat events in Southern California and contribution of Santa Ana Winds. *Environmental Research Letters*, 15 (5), 054017.

Si, M., *et al.*, 2022. Spatiotemporal pattern and long-term trend of global surface urban heat islands characterized by dynamic urban-extent method and MODIS data. *ISPRS Journal of Photogrammetry and Remote Sensing*, 183, 321–335.

Stewart, I.D., 2011. A systematic review and scientific critique of methodology in modern urban heat island literature. *International Journal of Climatology*, 31 (2), 200–217.

Stone, B., 2007. Urban and rural temperature trends in proximity to large US cities: 1951–2000. *International Journal of Climatology*, 27 (13), 1801–1807.

Streutker, D.R., 2003. Satellite-measured growth of the urban heat island of Houston, Texas. *Remote Sensing of Environment*, 85 (3), 282–289.

Turner, K.V., *et al.*, 2022. More than surface temperature: mitigating thermal exposure in hyper-local land system. *Journal of Land Use Science*, 17 (1), 79–99.
Unger, J., Sümeghy, Z., and Zoboki, J., 2001. Temperature cross-section features in an urban area. *Atmospheric Research*, 58 (2), 117–127.
Wan, Z., Hook, S., and Hulley, G., 2015. MYD11A1 MODIS/Aqua land surface temperature/emissivity daily L3 global 1km SIN grid V006 [Data set]. NASA EOSDIS Land Processes Distributed Active Archive Center. Available from: https://doi.org/10.5067/MODIS/MYD11A1.006 [Accessed 27 Jul 2024].
Wang, W., and Shu, J., 2020. Urban renewal can mitigate urban heat islands. *Geophysical Research Letters*, 47 (6), e2019GL085948.
Wang, Z., 2022. Reconceptualizing urban heat island: Beyond the urban-rural dichotomy. *Sustainable Cities and Society*, 77, 103581.
Xia, C., 2024. Escaping environmental hazards? Human mobility in response to air pollution and extreme cold events. *Annals of the American Association of Geographers*, 114 (6), 1268–1290.
Xia, C., Zhang, A., and Yeh, A.G.O., 2022. The varying relationships between multidimensional urban form and urban vitality in Chinese megacities: Insights from a comparative analysis. *Annals of the American Association of Geographers*, 112 (1), 141–166.
Xiang, Y., *et al.*, 2021. Seasonal variations of the dominant factors for spatial heterogeneity and time inconsistency of land surface temperature in an urban agglomeration of central China. *Sustainable Cities and Society*, 75, 103285.
Xu, Z., *et al.*, 2016. Impact of heatwave on mortality under different heatwave definitions: A systematic review and meta-analysis. *Environment International*, 89-90, 193–203.
Yang, K., *et al.*, 2022. RSEDM: A new rotational-scan exponential decay model for extracting the surface urban heat island footprint. *Remote Sensing*, 14 (14), 3505.
Yang, Q., *et al.*, 2023. An adaptive synchronous extraction (ASE) method for estimating intensity and footprint of surface urban heat islands: A case study of 254 North American cities. *Remote Sensing of Environment*, 297, 113777.
Yang, Q., Huang, X., and Tang, Q., 2019. The footprint of urban heat island effect in 302 Chinese cities: Temporal trends and associated factors. *The Science of the Total Environment*, 655, 652–662.
Yang, X., *et al.*, 2017. The urban cool island phenomenon in a high-rise high-density city and its mechanisms. *International Journal of Climatology*, 37 (2), 890–904.
Yao, R., *et al.*, 2019. Greening in rural areas increases the surface urban heat island intensity. *Geophysical Research Letters*, 46 (4), 2204–2212.
Yao, R., *et al.*, 2021. A robust method for filling the gaps in MODIS and VIIRS land surface temperature data. *IEEE Transactions on Geoscience and Remote Sensing*, 59 (12), 10738–10752.
Yao, R., *et al.*, 2023. Global seamless and high-resolution temperature dataset (GSHTD), 2001–2020. *Remote Sensing of Environment*, 286, 113422.
Yao, R., *et al.*, 2024. Estimation of the surface urban heat island intensity across 1031 global cities using the regression-modification-estimation (RME) method. *Journal of Cleaner Production*, 434, 140231.
Zhang, A., *et al.*, 2021. How can the urban landscape affect urban vitality at the block level? A case study of 15 metropolises in China. *Environment and Planning B: Urban Analytics and City Science*, 48 (5), 1245–1262.
Zhang, K., *et al.*, 2023. Increased heat risk in wet climate induced by urban humid heat. *Nature*, 617 (7962), 738–742.
Zhang, X., *et al.*, 2004. The footprint of urban climates on vegetation phenology. *Geophysical Research Letters*, 31 (12), L12209.
Zhang, Z., *et al.*, 2014. A 2010 update of National Land Use/Cover Database of China at 1: 100000 scale using medium spatial resolution satellite images. *Remote Sensing of Environment*, 149, 142–154.
Zhao, L., *et al.*, 2014. Strong contributions of local background climate to urban heat islands. *Nature*, 511 (7508), 216–219.

Zhao, L., *et al.*, 2018. Interactions between urban heat islands and heat waves. *Environmental Research Letters*, 13 (3), 034003.

Zhao, M., *et al.*, 2016. Influence of urban expansion on the urban heat island effect in Shanghai. *International Journal of Geographical Information Science*, 30 (12), 2421–2441.

Zhou, D., *et al.*, 2014. Surface urban heat island in China's 32 major cities : Spatial patterns and drivers. *Remote Sensing of Environment*, 152, 51–61.

Zhou, D., *et al.*, 2015. The footprint of urban heat island effect in China. *Scientific Reports*, 5 (1), 11160.